Practical implementation of Li doped SiO in high energy density 21700 cell

Y. Reynier, C. Vincens, C. Leys, B. Amestoy, E. Mayousse, B. Chavillon, L. Blanc, E. Gutel, W. Porcher, T. Hirose, et al.

Version of Record: https://www.sciencedirect.com/science/article/pii/S0378775320300021
Manuscript_c904a8ed4f76f866ff470e8431922b24

Practical implementation of Li doped SiO in high energy density 21700 cell

Y. REYNIER, C. VINCENS, C. LEYS, B. AMESTOY, E. MAYOUSSE, B. CHAVILLON, L. BLANC, E. GUTEL, W. PORCHER

Université Grenoble Alpes, CEA-LITEN, France

T. HIROSE, C. MATSUI

Shin-Etsu Chemical Co., Ltd, Japan

Abstract

SiO is a promising negative electrode material to increase Li-ion batteries specific energy thanks to its high capacity and stability. However it needs to be blended in low amounts with graphite because of its poor first cycle efficiency. Here we implement new Li doped carbon coated SiO material that overcomes this limitation and enables higher energy density cells. Reference SiO grade is compared to pre-lithiated materials and SiO content up to 20% blend with graphite are evaluated in pouch and 21700 cells with more than 500 cycles obtained at 90% depth of discharge. Reaction mechanism is proposed for standard as well as pre-lithiated SiO, and generalized for SiO_x. Finally we discuss behavior in hard casing full cell using this simple model to calculate volume expansion. We show with steric consideration that 40% SiO is likely the ultimate ratio practically usable in cylindrical cells.

Keywords

Li-ion; SiO; silicon oxide; 21700; pre-lithiation

1 INTRODUCTION

Since Li-ion batteries were first commercialized by Sony in 1991, the cell level specific energy increased from roughly 100 $Wh.kg^{-1}$ [1] to 250 $Wh.kg^{-1}$ [2,3] today. At the positive electrode lithium cobalt oxide is now challenged by nickel manganese cobalt layered oxides (NMC) as the leading material due to cobalt criticality [4]. In order to minimize cobalt content and increase material's capacity, today NMC622 is widespread and NMC811 cells is available in 18650 cells for electronics [5] as well as studied for next generation cells in automotive applications. On the negative electrode graphite in its natural or artificial

form has been the material of choice for more than twenty years [6] thanks to its outstanding stability, low volume expansion, high reversible capacity (372 $mAh.g^{-1}$ theoretical), small irreversible capacity [7] and low cost. In order to increase the energy density, silicon (with 3580 $mAh.g^{-1}$ theoretical capacity) has been researched and is now commercialized in the form of composites with graphite [8]. However due to its large volume expansion (up to 280% [9]) and first cycle irreversible capacity, it must still be blended in low amounts [5]. It is especially true for SiO materials, whose first cycle efficiency is usually below 75% [10,11]. Indeed SiO is supposed to be composed of nano clusters of Si and SiO_2 [12,13]. During electrochemical lithiation, SiO_2 domains irreversibly forms lithium silicate Li_4SiO_4, and a Si^{0+} plus other lower valence SiO reversible part [14,15,16]. It was also shown by NMR that when charged above 0.7V vs. Li, Li_4SiO_4 is reactive, which causes capacity fading [24]. Indeed this reversed reaction induces disproportionation and segregation of silicon domains [17] which then may behave as pure silicon with crystallization of $Li_{15}Si_4$ known for poor cycle life. If the number of lithium irreversibly trapped in the silicates is higher than the ones given by the positive electrode during the first cycle (around 11% irreversible capacity for NMC for example [18]) then the cell design does not use the full potential of the positive. As a consequence the cell's specific energy is not optimal.

To solve the large irreversibility issue of new negative electrode materials several pre-lithiation methods have been suggested [19]: direct contact of the negative electrode with Li metal [20,21], sacrificial salt oxidizing and releasing lithium in the positive electrode [22], protected Li powder mixed in the negative electrode slurry [16], or electrochemical pre-lithiation [23]. These methods pose several unresolved issues, rendering them largely impractical for industrial implementation: using thin and reactive lithium foil in large cells is a process challenge, sacrificial salts are often producing large amount of gas when decomposing and so called stabilized Li metal powder is still too reactive to be used with usual solvents. Finally ex situ electrochemical lithation of graphite or silicon gives rise to a highly reactive lithiated electrode that must then be further processed to a cell in an inert environment. Here new Li doped carbon coated SiO grades are evaluated (Li-SiO-C). Compared to the 72% efficiency with 1.2V vs. Li^+/Li cutoff voltage of the reference material [24], they attain up to 90% first cycle efficiency, without sacrificing the reversible capacity of around 1400 $mAh.g^{-1}$. Moreover they are stable enough to be processed in standard aqueous based slurries. This enables making full cells with large amount of Li-SiO-C compared to the state of the art, opening the way to very high energy density.

Next several optimizations are possible to get higher energy density at cell level. First lowering electrodes porosity enables packing more active material in the same volume and also increase the inactive/active

mass ratio (less electrolyte needed to fill pores). It is then favorable to reduce the inactive components volume and weight: using thinner separator and current collectors leads to increased performance. Finally active materials with higher specific capacity can be used. NMC 811 grades with capacity in excess of 200 $mAh.g^{-1}$ are now commercially available. Besides, in the final cell design the electrode loadings [25] and balancing will determine the resulting energy density. Those points will be explored in the discussion. Since a large proportion of silicon is needed in the negative electrode to reach high energy density, it raises concern about mechanical integrity in hard casing cells. Stress is known to develop in Li-ion cells because of active material swelling and solid electrolyte interphase (SEI) buildup in the negative electrode [26,27]. A part of the stress is reversible and cyclic, caused by variation of volume of active material during lithiation and delithiation [28], but stress also accumulate irreversibly [29]. Consequences of SiO volume expansion on cell design will be calculated and discussed.

The target of the development detailed below is a portable medical application. Specific energy of the power source is the primary concerns since the device is to be used by a very weak patient in hospital environment. Safety is another critical aspect which leads to the 21700 hard casing design with built in multiple safety devices (dual vents, CID, ceramic coated separator).

2 EXPERIMENTAL

2.1 SIO-C MATERIAL SYNTHESIS

A mixture of silicon dioxide (Shin-Etsu Chemical Co., Ltd, Purity 99.9%, Size D50 = 10 µm) and silicon (Shin-Etsu Chemical Co., Ltd, Purity 99%, Size D50 = 10 µm) was vaporized in a reactor at 10 Pa and 1340 °C, then cooled and accumulated on a plate as silicon-monoxide (SiO). The SiO bulk was pulverized by milling to make the SiO powder with around 6.5 µm median particle size. It was then processed for 3 h in methane at ca. 1000 °C to make a conductive carbon coating of around 30 nm thickness on the powder surface (SiO-C).

2.2 ELECTRODES FABRICATION

Electrodes were coated using a standard slurry method, with NMP solvent on 20 or 15µm thick aluminum current collector for the positive and water solvent on 10µm thick copper current collector for the negative. The positive electrode consisted of 94.5%wt commercial grade NMC active material (532, 622 or 811), carbon conductive additive and PVDF binder (SOLVAY). Negative electrode was composed of artificial

graphite active material, carbon coated SiO (Shin Etsu Co.), carbon conductive additive, CMC thickener (Aldrich) and SBR binder (BASF). The active material content (including graphite and SiO) was set to 91%wt. A custom reverse roll coater installed in dry room with 1.5m drying oven was used for both electrodes.

2.3 CELLS FABRICATION

The capacity and the charge-discharge curve of the SiO-C anode materials were measured using a 2032-type coin cell with metallic Li as the counter electrode and 1.2 M $LiPF_6$, 0.1 M $LiBF_4$ EC:FEC:DMC = 25:5:70 (vol.%) as the electrolyte.

Pouch cells were used to evaluate cycle life: they were assembled in a -20°C dew point dry room with one single layer positive electrode (3.2x3.2cm active area), a separator (Celgard 20µm, ceramic coated) and an oversized negative electrode (3.5x3.5cm). After drying under vacuum at 55°C they were transferred in an argon atmosphere glove box for electrolyte filling with $LiPF_6$ 1M in EC:DMC:EMC (1:1:1 vol) + 5%wt FEC. In order to validate performance and energy density, 21700 cylindrical cells were produced using the same separator and electrolyte as the pouch cells.

2.4 ELECTROCHEMICAL CHARACTERIZATION

Coin cells evaluation was conducted under the following conditions: current rate of 0.2 mA/cm^2, constant current and constant voltage charging, and constant current discharging.

Pouch and 21700 cells were tested using PEC Corp. and Arbin cyclers. They were first formed at 45°C using a constant current constant voltage (CCCV) C/20 charge between 2.5 and 4.2V with C/50 minimum current at end of charge and a C/20 constant current discharge down to 2.5V.

Pouch cells discharge rate capability was evaluated at room temperature with 0.2, 0.4, 0.6, 0.8 and 1C rate using a C/5 CCCV charge up to 4.2V until current drops below C/20. Standard cycling was carried out at room temperature and C/5 (with CCCV down to C/20 at the end of charge), using a [3-4.2V] voltage window, corresponding to approximately 90% depth of discharge compared to 2.5V cutoff. For 21700 cells, discharge rate capability was evaluated at C/3 C/2 and 1C, then resistance was measured during discharge every 5% SoC with a 30s 2C pulse. Cycling on 21700 was made with C/5 charge (CCCV 4.2V, C/20) and C/3 discharge down to 3V.

2.5 ^{29}Si NMR CHARACTERIZATION

The measuring equipment was a Bruker Avance700 operating at the observation frequencies of 139 MHz (Si). The measurement method was comprised of a single-pulse irradiation under MAS with an irradiation pulse intensity of 30° and relaxation times of 30 s. The scan numbers were 12,000. LiCl was used as a secondary standard for the chemical shifts, and its shift value was obtained from 1 M LiCl.

3 RESULTS

The different SiO-C grades studied in the present work are described in Table 1 : Grade A is the reference non pre-lithiated, carbon coated material. Detailed characterization of this grade can be found in previous literature [17,24]. Grade B and C have different levels of lithium doping [30,31], resulting in better first cycle efficiency (Figure 1).

Reference	**Grade denomination**	**Density / g.cm^{-3}**	**Discharge capacity / mAh.g^{-1}**	**Charge capacity / mAh.g^{-1}**	**1st cycle efficiency / %**
KSC-1265	A	2.27	2212	1560	70.5
KSC-7125	B	2.35	1666	1425	85.5
KSC-7130	C	2.34	1544	1395	90.3

Table 1: 1st cycle Coin cell performance vs. Li of the SiO-C grades [0-1.2V] CC-CV

Initial lithiation voltage of grade A is much lower than Li-doped materials: irreversible silicates formation has already been partially performed during the synthesis for these grades. As a result the first discharge capacity is smaller. Differential capacity plot (Figure S3) shows a large reduction peak for grade A, which could be assigned to Li_4SiO_4 formation seen by NMR in the same range [17]. It is much less pronounced for grade B and C and a new peak appears at higher voltage (112 instead of 65 mV) which indicates different reduction mechanism for the prelithiated materials. Delithiation however is very similar for the three grades (see also Figure S3) and comparable to the literature [40,46,60] with two peaks at 300 and 500 mV .The same peaks are also seen for pure silicon [60], hinting at the same delithiation mechanism for Si and the three SiO grades after first discharge. Small peaks around 100mV may be attributed to lithium extraction from carbon conductive additive at low voltage [40].

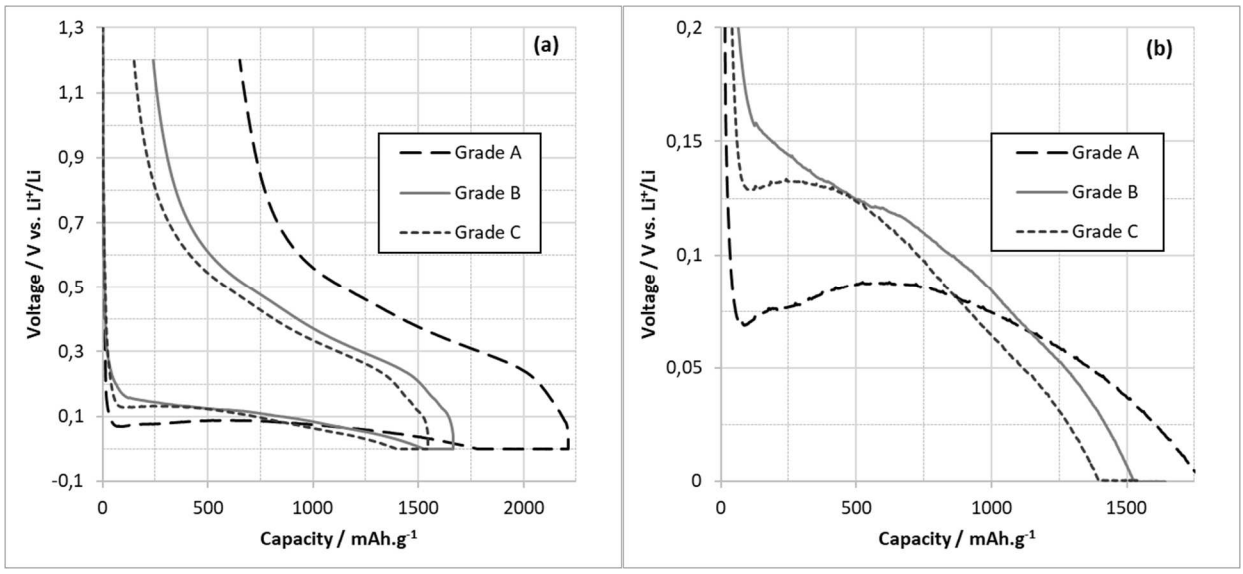

Figure 1 : (a) First discharge-charge cycle for the different SiO-C grades in coin cells vs. Li, (b) low voltage region of the first discharge

Grade C has enough pre-lithiation to reach more than 90% first cycle efficiency, a value similar to standard graphite [7], and matching the one of NMC in order to use its full capacity. Indeed the capacity of a cell is calculated as: $Q_{cell} = \min(Q_{tot}^{+}, Q_{tot}^{-}) - \max(Q_{irrev}^{+}, Q_{irrev}^{-})$, where Q_{cell} is the usable cell capacity, Q_{tot}^{+} the positive electrode total capacity during first charge, Q_{tot}^{-} the total negative electrode capacity during first discharge vs. lithium, and $Q_{irrev}^{+/-}$ the positive or negative first cycle irreversible capacity vs. lithium. Q_{tot}^{-} is always larger than Q_{tot}^{+} to prevent Li plating during the first cycle. When Q_{irrev}^{-} becomes larger than Q_{irrev}^{+}, full cell's capacity is lower than what the positive electrode can deliver.

^{29}Si NMR was performed on pristine grades A, B and C (Figure 2): The standard grade appears as a mixture of crystalline silicon (c_Si) (-85ppm) and SiO_2 (-110ppm) [17]. In the lithium doped Grade B material, SiO_2 peak has nearly vanished at the expense of two new phases which can be indexed as lithium silicates [46]: Li_2SiO_3 (-75ppm) and $Li_2Si_2O_5$ (-93ppm). Surprisingly for grade C only Li_2SiO_3 can be spotted. The bump centered at -60ppm could be attributed to some amorphous silicon or low valence silicon formed along the silicates. This suggest a different reaction path for the three grades: during Li pre doping some Li silicates are formed, which account for half (grade B) or two third (grade C) of grade A irreversible capacity (see also patents [30,31]). In grade C, SiO_2 peak has completely disappeared, suggesting a complete conversion into silicates.

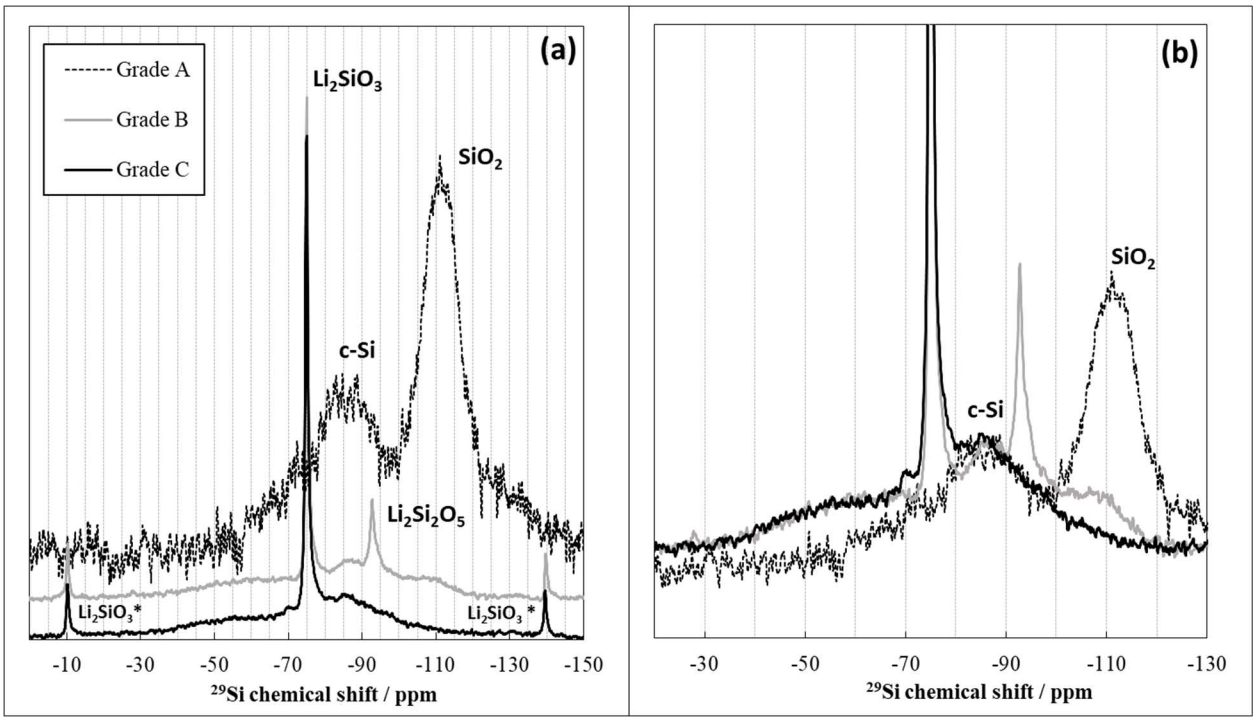

*Figure 2 : ^{29}Si NMR of the pristine SiO-C grades (a): full spectra (b): normalized insert. *: spinning side bands*

In order to determine the best electrode loading for the targeted application three series of pouch cells were assembled: one with a positive electrode at 21 mg.cm^{-2} (low loading LL), one at 27 mg.cm^{-2} (medium loading ML) and a last one at 33 mg.cm^{-2} (high loading HL). Negative electrode consisting of 5% SiO-C mixed with graphite were matched for each loading. Specifications of each series of pouch cells is summarized in Table 2.

Pouch cells Reference	Positive electrode active material	Negative electrode SiO content / %wt	Pos. electrode loading / mg.cm^{-2}	Neg. electrode loading / mg.cm^{-2}	1st cycle efficiency / %
LL	NMC532	5% Grade A	21	10.3	82.4
ML	NMC532	5% Grade A	27	14.4	81.5
HL	NMC532	5% Grade A	33	16.2	82.6

Table 2 : specification of pouch cells for loading study

Capacity retention during C/5 cycling in the [3-4.2V] voltage window is shown on Figure 3. Very similar trends are observed for all the loadings, indicating that it has not a major influence in the range studied (21-33 mg.cm^{-2}). After 300 cycles all pouch cells fall within 5% of each other's. LL and HL cells were cycled up to 600 cycles where they lose 22% capacity. As expected, the fading rate is higher than state of the art NMC/graphite cells. For instance Gallagher using similar NMC622 with loading of 31 mg.cm^{-2} in 14

cm² pouch cells achieved less than 3% capacity loss after 283 C/3 cycles [25]. However considering the 5% SiO-C content in the negative electrode and high loadings this performance compares favorably to the literature [32,33], and commercial LG MJ1 18650 cell containing ~5% Si in the negative electrode [34].

Such fading can be explained by negative SEI growth and particle cracking [34]. SEI on the surface of SiO is composed of alkyl carbonates, Li_2CO_3, methyl silane and phosphorus fluoride compounds [35]. K.W. Kim proposed a mechanism for aging of silicon monoxide containing anodes [36]: SiO volume expansion causes particle cracking, exposing new surface to the electrolyte. The new SEI formed irreversibly consumes the lithium inventory of the cell. It also gradually increases the cell's resistance causing more fading. This mechanism is similar to the one of silicon containing electrodes [37] although less pronounced because SiO volume expansion is less than half the one of silicon [60].

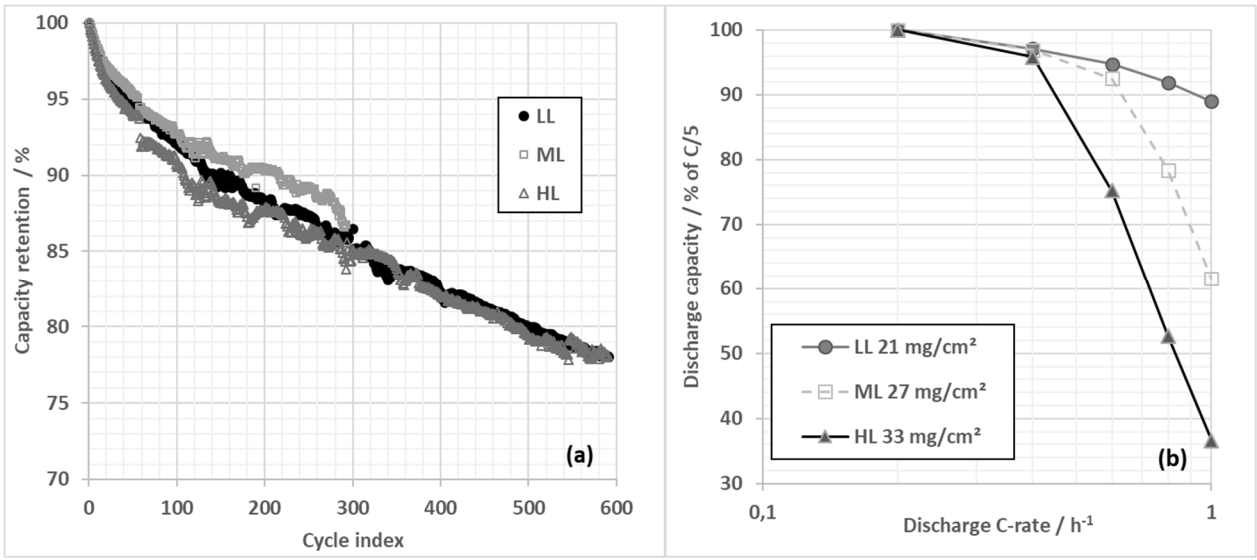

Figure 3 : effect of electrode loading, (a) Capacity retention of LL, ML and HL pouch cells during C/5 cycling [3-4.2V] corresponding to 90% DoD normalized to 100% capacity at C/5 and (b) discharge rate capability

Rate capability results of LL, ML and HL pouch cells are shown on Figure 3b. It is well known that electrode loading is one of the primary limiting parameter for rate capability [38]. Indeed in thick electrodes when the discharge C-rate increases, the lithium ion concentration can fall to zero in the depth of the positive electrode (close to the current collector), leading to under-utilization of the active material. Here the LL electrode allows for nearly full utilization up to 1C (90% capacity retention) when the ML cells are only able to deliver 60% capacity and the HL 35% at this rate. However for targeted discharge times longer than two hours, the HL cells still deliver near full capacity. As a consequence the highest loading

was selected for further optimization. It is worth noting that when discharge rate is normalized in mA per square cm of electrode area (Figure S1), all the cells achieve the same capacity around 3.5 $mA.cm^{-2}$.

The effect of increased SiO-C content is shown on Figure 4 using the same NMC532 positive electrode at 33 $mg.cm^{-2}$. With 10%wt SiO-C the cycle life trend is the same as 5%wt, but as seen in Table 3, due to the large first cycle irreversible capacity of grade A, the initial reversible capacity is lower. This illustrates that high SiO-C content will not necessarily increase the energy density if pre-lithiation is not used. Indeed, with the grade B which has 85% 1st cycle efficiency, the pouch cell irreversible capacity is only 12.4% when mixed with graphite (Table 3) at 10%wt leading to improved cell capacity, without degrading the cycle life as shown on Figure 4a. While increasing the SiO-C content is not always beneficial to full cell capacity, it can have a positive effect on cell manufacturing and rate capability: Going from 5 to 10% SiO-C with the same cathode loading enables a decrease of negative electrode loading from 16.3 $mg.cm^{-2}$ to 14 $mg.cm^{-2}$ and electrode thickness from 103 to 89 µm. As a result rate capability is slightly increased (Figure 4b) and electrode manufacturing eased.

Positive AM	**SiO-C content in the negative**	**Charge capacity / mAh.g^{-1} of positive AM**	**Discharge capacity / mAh.g^{-1} of positive AM**	**1st cycle irrev. / %**
NMC532	5% grade A	195.5	161.5	17.4
NMC532	10% grade A	193.0	154.3	20.0
NMC622	10% grade B	195.9	171.7	12.4
NMC622	20% grade C	195.3	173.3	11.3

Table 3: formation results of pouch cells with different SiO-C contents and grades in the [2.5-4.2V] window

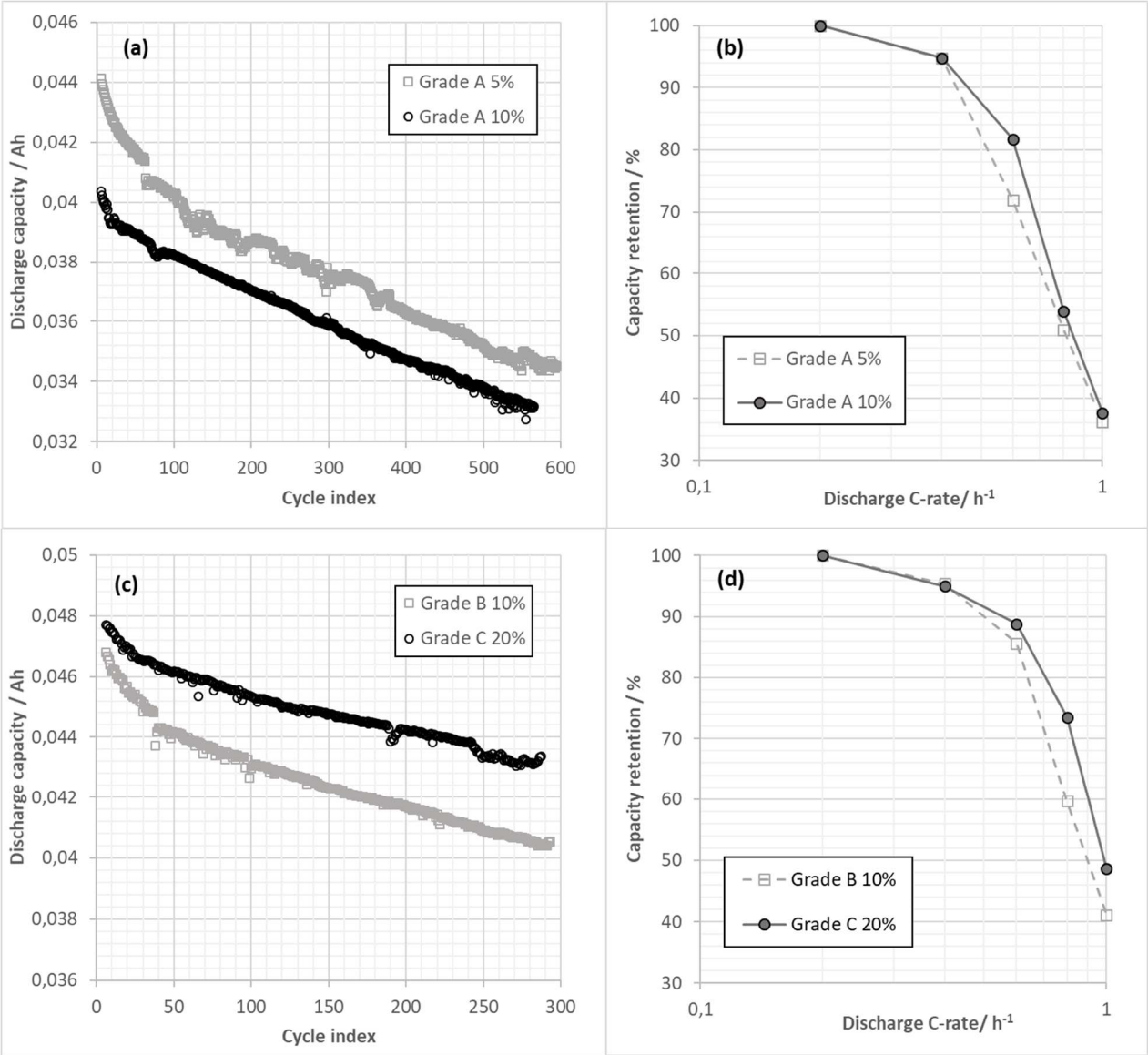

Figure 4: Discharge capacity during C/5 cycling [3-4.2V] for pouch cells with (a): NMC532 positive electrode vs. grade A at 5 and 10%wt mixed with graphite, (b): rate capability of the same cells, (c) 10% grade B or 20% grade C mixed with graphite vs. NMC622 positive (34mg.cm^{-2}), (d) rate capability of the same cells

Thanks to a higher level of prelithiation, grade C enables a 20% Li-SiO-C level in the negative electrode without sacrificing the full cell reversible capacity, as shown on Table 3. Actually the 173 mAh.g^{-1} recovered during first discharge corresponds to the maximum possible capacity of the NMC622 material for a 4.2V cutoff voltage. It means that in this case the irreversible capacity of the positive electrode is higher than the negative electrode. Capacity retention shown on Figure 4c is better for grade C at 20% in graphite than grade B at 10% in graphite. This may be due to the extra lithium inventory provided in the cell thanks to prelithiation: the excess lithium available after negative electrode initial passivation might be able to compensate for lithium loss during cycling. Since loading of the negative electrode is even lower

with 20% Li-SiO-C to match the same positive loading of 34 mg.cm^{-2} (5.8 mAh.cm^{-2}), going down from 15 mg.cm^{-2} to 12 mg.cm^{-2}, rate capability is enhanced.

21700 cells were assembled with a negative electrode formulation containing 70%wt graphite and 20%wt Li-SiO-C grade C as the active materials. Positive electrode consisted of NMC622 with 29 mg.cm^{-2} loading. Electrode balancing is set to 1.1 and cells average weight is 63.8g. 4.2 Ah is obtained during formation's C/20 discharge, corresponding to 230 Wh.kg^{-1}, with 11.3% average first cycle irreversible capacity. Rate capability during discharge is shown on Figure 5: the capacity is stable up to 1C, thanks to heating effect at higher rate compared to small and thin pouch cells, which increases electrolyte conductivity. Pulse power performance is composed of two distinct areas: above 55% SoC, the resistance is more or less flat with two plateaus at around 55 mΩ, then it increases continuously up to about 100 mΩ. Considering the Li-SiO-C content the negative electrode capacity can be calculated at 578 mAh.g^{-1}, of which 299 mAh.g^{-1} is brought by silicon oxide. During discharge because of the potential difference between silicon oxide and graphite, the latter is delithiated first, so the first zone can be attributed to graphite and the capacity ratio fits well. Then at SoC lower than 50% SiO is delithiated: it appears then that grade C Li-SiO-C might bring slightly higher resistance than graphite.

Cycle life of the 21700 cells with C/5 charge and C/3 discharge is compared to pouch cells cycling at C/5 in the same [3-4.2V] voltage window (Figure 5): fading trend is very similar indicating a successful scale up to prototype cells. Initial capacity of 21700 cell for this 90% DoD test is 3475 mAh.

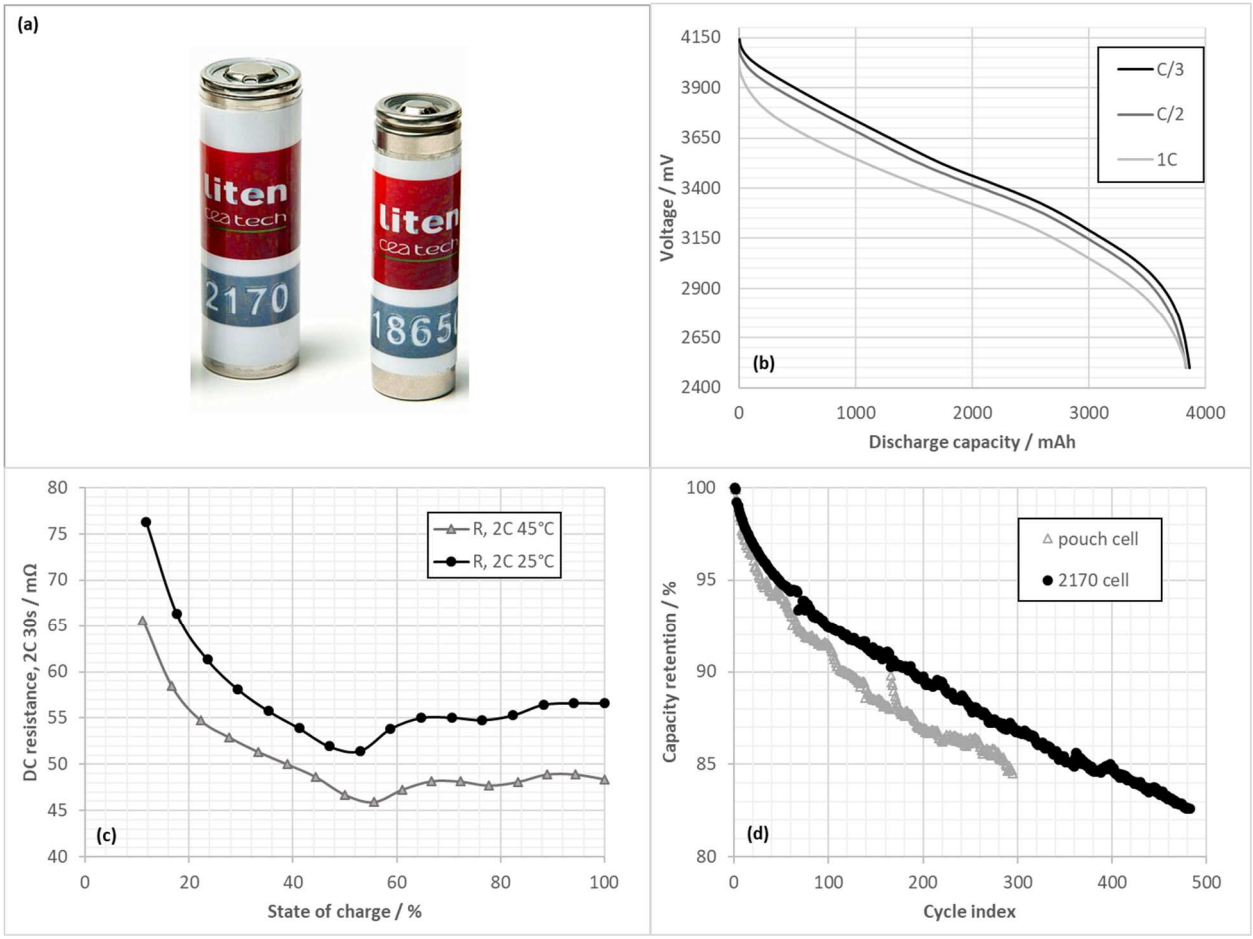

Figure 5 : 21700 cells performance. (a) Cell size compared to 18650 (b) rate capability (c) Resistance vs. SoC at 25 and 45°C (d) cycle life at C/3 discharge rate compared to pouch cell (cycling C/5) [3-4.2V]

4 DISCUSSION

Possible optimizations to increase specific energy are summarized in Figure 6: 21700 cell performance is calculated with in house CEA tool used to design Li-ion cells, taking into account all the components physical properties, and active materials specific capacities. Stars symbolize three experimentally tested designs: the first one is presented in Figure 5. It use 30% positive electrode porosity, 35% negative electrode porosity and conservative Al current collector and separator, both 20 µm thick. The second design uses NMC811 and thinner 15µm Al current collector. Measured initial performance at C/20 is 255 $Wh.kg^{-1}$. With thinner separator (16 µm) and lower balancing (5.1 $mAh.cm^{-2}$ positive electrode, keeping same 6 $mAh.cm^{-2}$ negative) it is possible to reach 4.9 Ah and 267 $Wh.kg^{-1}$ (715 $Wh.L^{-1}$) at C/20 for the last tested 21700 design.

Figure 6b illustrates the influence of Li doped SiO-C on full cell specific energy: contrary to standard grade A where it is levelling off above ~5% SiO-C because of low 1st cycle efficiency, with grade C the performance optimum would theoretically be 100% Li-SiO-C.

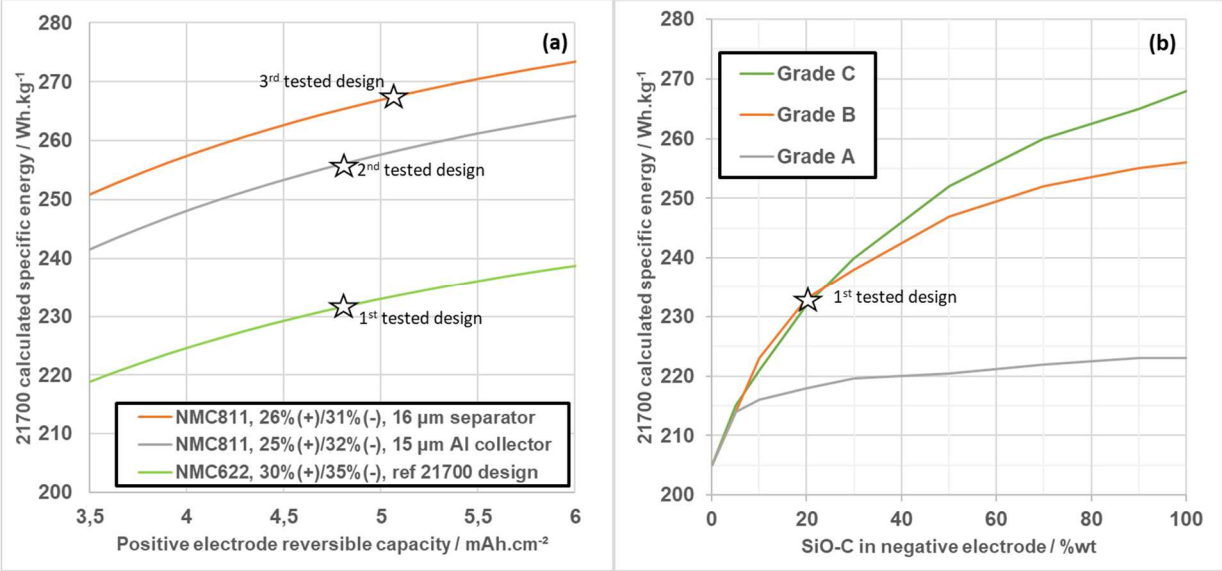

Figure 6 : Cell level specific energy density calculations (a): influence of various optimizations (b) with constant 4.8 mAh.cm^{-2} NMC622 positive and variable SiO-C content in negative electrodes. Stars show tested design in 21700

Using 100% grade C in the third 21700 tested design would theoretically allow to pass the 300 Wh.kg^{-1} mark. However in this case, serious concerns can be raised regarding silicon volume expansion in a hard casing design. The following calculations aim to evaluate this value.

In SiO, the Li-Si alloy does not crystallize in the form of $Li_{15}Si_4$ contrary to what happens with pure silicon [39, figure S2]. NMR studies evidenced a maximum lithiation y in Li_ySi between 3.25 ($Li_{13}Si_4$) [15] and more recently 3.44 [40]. A simplified mechanism for SiO_2 reaction can be postulated as follows:

$$2SiO_2 + 4(Li^+ + e^-) \rightarrow Si + Li_4SiO_4 \quad (1a)$$

$$3SiO_2 + 4(Li^+ + e^-) \rightarrow Si + 2Li_2SiO_3 \quad (1b)$$

$$5SiO_2 + 4(Li^+ + e^-) \rightarrow Si + 2Li_2Si_2O_5 \quad (1c)$$

$$SiO_2 + 4(Li^+ + e^-) \rightarrow Si + 2Li_2O \quad (1d)$$

$$3Li_2Si_2O_5 + 4(Li^+ + e^-) \rightarrow Si + 5Li_2SiO_3 \quad (2)$$

$$Si + y(Li^+ + e^-) \leftrightarrow Li_ySi \quad (3)$$

In Grade A, previous literature suggest reaction 1a occurs predominantly, while for grade B reaction 1b and 1c seem to take place before first electrochemical lithiation as evidenced by our NMR results. In Grade C we postulate that upon further Li pre-doping reaction 2 takes place. Li_2O may also be formed, although we couldn't get clear evidence of its presence in the bulk in our previous study using NMR [17]. The difficulty resides in the fact that Li_2O chemical shift (near 3ppm, based on tin oxide reaction study [41]) is overlapping with lithium silicate Li_4SiO_4 and possible electrolyte reduction products. Li_2O has been spotted by X-ray techniques (XAFS, XPS) [42,43]. However lithium carbonate that can be found in the SEI (resulting from carbonate electrolyte reduction during formation) has been shown to react very quickly to form Li_2O under soft X-ray irradiation [44]. This suggest particular care must be taken when analyzing sample results using such techniques. In the following simplified model we will not consider Li_2O: taking it into account would change slightly volume calculations (we calculated 10% more expansion for SiO if one third of irreversible capacity is coming from Li_2O, has proposed by ref. 45), since its density of 2.0 $g.cm^{-3}$ [48] is lower than silicates.

Using $2SiO \sim Si+SiO_2$ identity, the following overall reaction can be derived by combining 1a and 3 for the standard grade A:

$$4SiO + (4 + 3y)\,(Li^+ + e^-) \rightarrow Li_4SiO_4 + 3Li_ySi \qquad (4a)$$

With this equation and values summarized in Table 4, capacities and volume expansion of fully lithiated material can be calculated as a function of *y* (Table S1). SiO density has been reported between 2.13 [12] to 2.18 [46], which is lower than density of both amorphous Si (2.29) and SiO_2. However density was measured at 2.27 for grade A, which nicely fits a linear regression between c_Si and SiO_2.

phase	$g.mol^{-1}$	$cm^3.mol^{-1}$	$g.cm^{-3}$	$Ah.mol^{-1}$	$mAh.g^{-1}$ of AM	expansion / %vol	Ref. for density
$Li_{15}Si_4$	216.5	183.6	1.18	402.1	3579	281	9
Li_2SiO_3	90.0	35.6	2.53	53.6	705	195	47
Li_4SiO_4	119.9	49.5	2.42	107.2	1164	152	48
c_Si	28.1	12.1	2.33				
a_SiO_2	60.1	27.3	2.20				13
SiO	44.1	17.5	2.27				

Table 4 : values used for capacity and volume expansion calculations.

We can see that the value of *y* closest to actual grade A performance (Table S1) fits well with the 3.44 reported in ref 40. Here depending on y value for maximum silicide stoichiometry, its molar ratio vs. irreversible part would evolve from 3 for y=3.75 to 2.6 for y=3.25, changing the calculated irreversible capacity of SiO-C.

While Li_4SiO_4 is mainly formed in standard SiO-C like grade A, in Li-doped SiO-C grades B and C, Li_2SiO_3 appears preferentially during Li pre-doping. In this case, taking into account that reaction (1b) gives rise to amorphous silicon (a_Si) as evidenced by NMR, the mechanism could be written as:

$$\left\{\frac{1}{2}a\_Si + Li_2SiO_3 + \frac{3}{2}c\_Si\right\} + (2 + 2y)\,(Li^+ + e^-) \leftrightarrow\ Li_2SiO_3 + 2Li_ySi \qquad (4b)$$

Lower reversible capacities measured for Li-doped grades B and C can be explained by their initial lithium content, adding weight to the compounds. Li-SiO-C already contains a maximum of 2/3 mol of Li (*3SiO* gives *½ a_Si + Li_2SiO_3 + 3/2 c_Si*, eq. 4b) accounting for 4.63 g.mol^{-1} vs. 44.1 g.mol^{-1} for initial SiO-C. This lowers specific capacity: using 1560 mAh.g^{-1} as reference capacity (grade A), this leads to a calculated value of 1411 mAh.g^{-1} for pre-doped materials, close to the 1395 mAh.g^{-1} actually measured for grade C.

However as evidenced by the 10% irreversible capacity still measured with grade C, accounting for one third of grade A first cycle loss, the pre doping process is only partial. The theoretical composition of pre-lithiated material such as grade C would be 1/6 a_Si+1/2 c_Si+1/3 Li_2SiO_3 per initial SiO formula. Since the silicates density is higher than the one of SiO, the density of grade B and C are higher than SiO. However the measured value of 2.35 for grade C, is not as high as the value calculated at 2.45 g.cm^{-3} based on (4b). This discrepancy can be attributed to partial pre-doping. It must also be noted that Li_2SiO_3 silicate density reported in Table 4 is quite old data, and recent simulations and experiments tend to find lower density in the range of 2.4 to 2.5 g.cm^{-3} [49, 50].

Then for SiO_x we attempt to generalize the reaction mechanism of equation 4a leading to eq. 5, 6 and 7:

$$SiO_x \sim \frac{2-x}{2}\,\mathrm{Si} + \frac{x}{2}\,SiO_2 \qquad 0 < x < 2 \qquad (5)$$

$$\frac{x}{2}SiO_2 + x(Li^+ + e^-) \rightarrow \frac{x}{4}Si + \frac{x}{4}Li_4SiO_4 \qquad (6)$$

$$\frac{2-x}{2}\mathrm{Si} + \frac{2-x}{2}y(Li^+ + e^-) \leftrightarrow \frac{2-x}{2}Li_ySi \qquad (7)$$

By combining eq.5, 6 and 7 and ensuring preserved stoichiometry, the overall mechanism can be written as:

$$4SiO_x + [4x + (4-x)y](Li^+ + e^-) \rightarrow xLi_4SiO_4 + (4-x)Li_ySi \quad (8)$$

In eq. 8, 4x lithium are irreversibly consumed forming silicates and the rest is reversible. From this equation and values summarized in Table 4, capacity of SiO_x and volume expansion can be calculated as a function of x.

However some uncertainty still remains in the densities values, since SiO is composed of more or less amorphous domains and it is not completely clear if the starting and end products are crystalline and in which allotrope. For instance Si crystalline density is 2.33, while amorphous Si as a density of 2.29. SiO_2 exist in a variety of allotropes ranging from quartz (2.65 $g.cm^{-3}$) to amorphous at 2.2. According to ref. 13, nano clusters of SiO_2 are crystalline and Si clusters amorphous in SiO. In ref. 24, crystalline Si is seen by XANES. Our NMR results suggest crystalline Si for pristine material. Thus in the following calculation, SiO-C starting material will be considered as a mixture of crystalline Si and amorphous SiO_2. As a consequence, a simple linear regression $d(x) = 2.332-0.065x$ was used to approximate the density of SiO_x as a function of x.

It must be also noted that these calculations only take into account the structural irreversible capacity, and it is known that some passivation will occurs also on the surface of SiO_x in presence of electrolyte, the amount of which will depend on the area and chemical nature of the surface. Since it takes place mainly at potential of approx. 0.8V in carbonate, it can be easy to spot compared to the Li insertion taking place below 0.5V [46]. For instance Kim [46] measured 150 $mAh.g^{-1}$ out of 1210 caused by passivation, which roughly is 12% more irreversible capacity.

Capacity of SiO is still controversial, and varies widely depending on the synthesis method (from ~700 to 1900 $mAh.g^{-1}$ [10]). The same is true for SiO_2 ranging from ~300 to 1400 $mAh.g^{-1}$, although always with large irreversible capacity of more than 30%.These apparently contradictory results may come from the better reactivity of the materials at nano size, but in this case large parasitic reaction can take place. Recently Flavors et al. [51] synthetized SiO_2 nanotubes and could get around 1000 $mAh.g^{-1}$ at 1V charge, with a 2500 $mAh.g^{-1}$ first discharge (of which ~800 $mAh.g^{-1}$ can be attributed to passivation).

Synthesis of SiO_x with variable value of x has been studied with model electrodes [52;53;54;55;56;57]. Table S2 summarizes the performance of SiO_x films as a function of x in five reports which used the same

sputtering process to make thin films. This method is interesting since no additive is present in the electrode and the active surface in contact with electrolyte is low, minimizing the effect of passivation.

One last uncertainty point comes from maximum lithiation ability of silicon domains in SiO: as mentioned earlier y=3.44 in Li_ySi seems to be the maximum value obtained for SiO, while for pure Si it can go up to $Li_{3.75}Si$ during electrochemical lithiation. This phase is still seen for composition up to x=0.17 [54], and pure Si behavior is preserved up to at least x=0.48 [53]. Al-Maghrabi et al. [57] who evaluated various SiO_x ratio and made a model postulating Li_4SiO_4 and $Li_{3.75}Si$ formation found a good fit up to the highest composition (x=0.67) they tested. In our model we thus postulate that composition $L_{15}Si_4$ is obtained up to x=0.65, then y=3.44 is used for x>0.7.

Good agreement is found between this crude model and literature data for the first charge capacity (Figure 7). Regarding first discharge (lithiation), a constant offset of about 100 $mAh.g^{-1}$ is observed. It may come from electrode passivation by electrolyte (forming Li_2O, Li_2CO_3, alkyl carbonates [58]) that is not taken into account by the model. This gives good confidence into the calculated volume expansion for SiO-C.

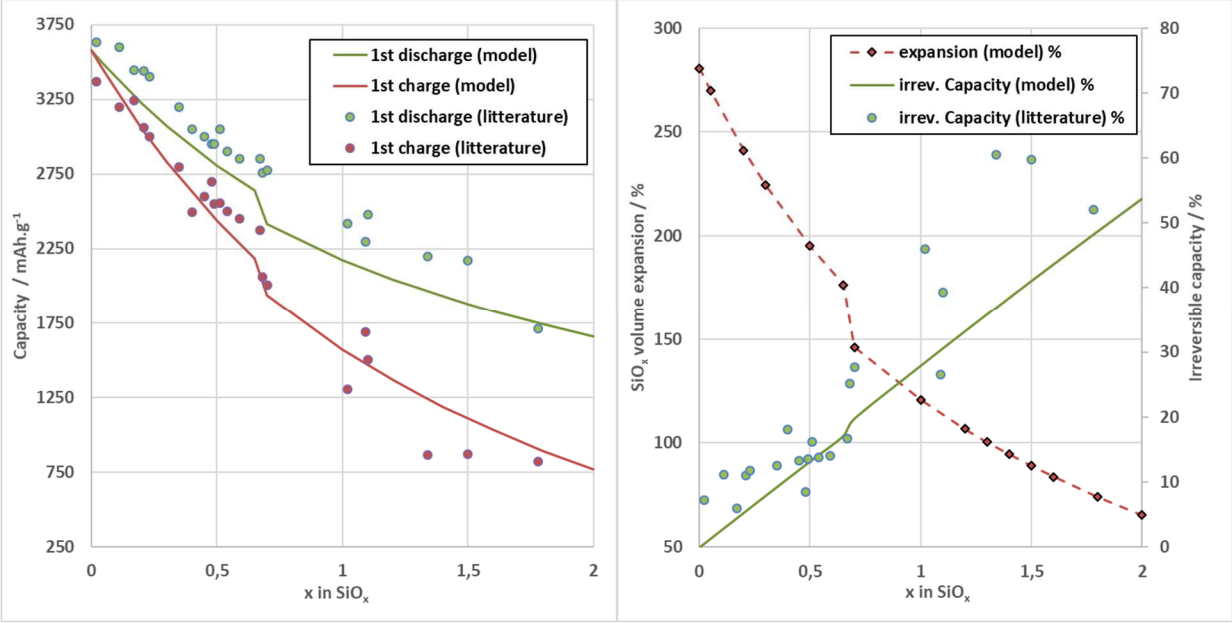

Figure 7 : (a) SiO_x first cycle charge and discharge capacities calculated with model compared to literature values (Table S2), (b) calculated volume expansion and irreversible capacity compared to literature values

Considering a 10% volume expansion for graphite and calculated 121% for SiO-C (which fits well with ref [59] and 118% expansion measured on SiO particle in [60]), when an electrode containing 20% SiO-C is fully charged, its volume should increase by nearly 32%. Since a 21700 cell has a constant internal volume, its components have to accommodate this expansion. A first possibility is for the porosity of the

negative electrode to go from initial value of 35% to 18%. Otherwise another component has to be compressed. Electrolyte can be considered incompressible in the relevant pressure window of the cells (less than 2.5 MPa bars before the safety vent opens).The polyolefin separator has a 50% internal porosity, but it will not compress a lot : A pressure of 6.9 MPa results in a mere 1 µm thickness variation on a standard Celgard 2500 polypropylene film [61]. Positive electrode is already calendared at high pressure (400 MPa),. Fortunately, NMC622 crystal structure contracts by about 3% when charged to 4.3V vs. Li [62], which could induce up to 6 µm thickness reduction of the positive electrode from the initial 212 µm of the tested design. In this regards NMC811 would even be better suited with 5% volume reduction in the same voltage window.

Calculated components volumes of 21700 cells with different Li-SiO-C content are compared in Table S3 keeping same NMC622 positive electrode and considering the slight volume change of positive electrode and expansion of negative electrode.

Figure 8 illustrates calculated components volume variation when cell is fully charged. By design the initial total volume of internal components is the same for all Li-SiO-C contents. The 20% SiO case corresponds to 21700 design whose performance is shown on Figure 5.

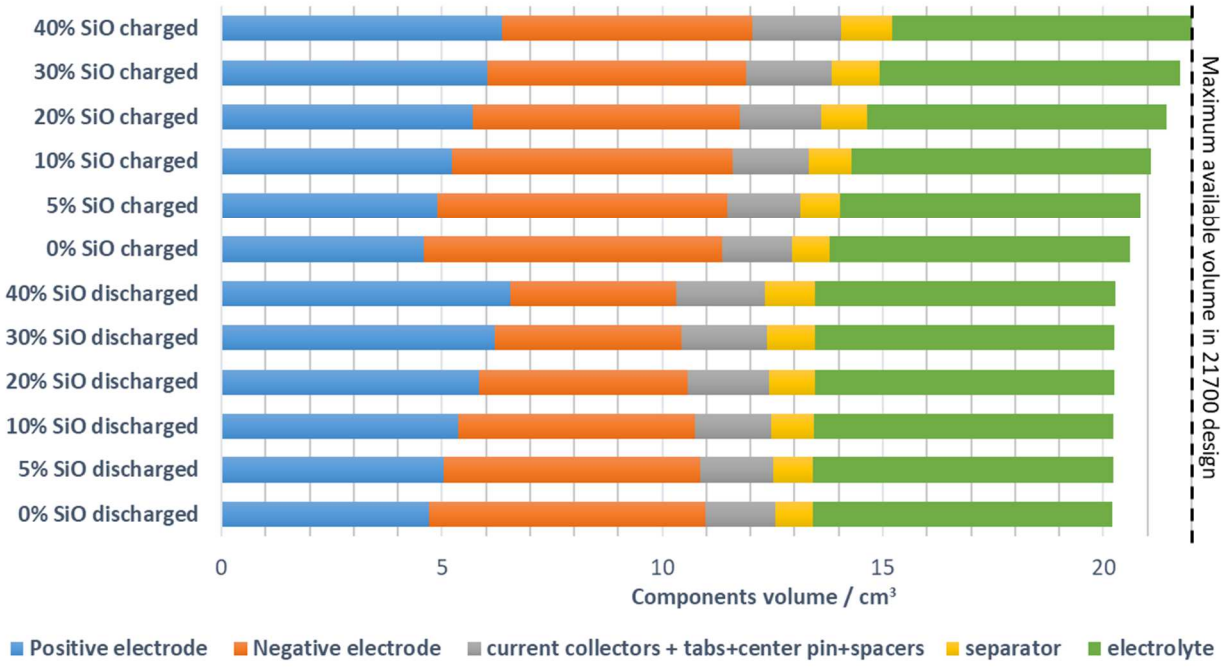

Figure 8: Influence of Li-SiO-C content on charged 21700 cell internal volume

First it can be seen that most of the space (86%) is taken by electrodes and electrolyte. Initial dead volume in the cell (left for gassing during cell life) is about 8%. In the fully charged cell with 20% Li-SiO-C anode it goes down to 0.54 cm^3.

With 30% Li-SiO-C in the negative electrode a volume increase of nearly 42% is expected upon charge. To accommodate this expansion, at 35% initial porosity a charged negative electrode porosity would have to go down to 15%, a value quite difficult to get with standard electrode calendaring process. It means high mechanical stress would probably develop in the cell. High stress is known to cause faster capacity fading [26] and ultimately cell failure by delamination and wrinkling of the jelly roll [63,64].

Pressure build up calculated using remaining dead volume when fully charged could go up to +7 bar (1.73/0.26), still lower than the venting pressure (18 bar) but quite high for beginning of life.

Same calculation with 40% Li-SiO-C negative electrode indicates that dead volume would go down to 0 cm^3 when charged, causing unacceptable pressure increase inside the cell. As a consequence less than 40% SiO is likely the ultimate limit in this 21700 design.

Finally it must be realized that increasing the initial negative electrode porosity wouldn't solve this issue, since it needs to be filled with electrolyte before the first charge in order for the cell to work properly: as a consequence initial dead volume in the cell would remain unchanged.

5 CONCLUSIONS

Li doped SiO-C enables manufacturing of high energy density Li-ion cells thanks to lower first cycle irreversible capacity while keeping good cycle life. Up to 20% Li-SiO-C / graphite blend was successfully implemented in industrially representative 21700 cells with 230 $Wh.kg^{-1}$ and more than 500 cycles proven at 90% DoD. A reaction mechanism was proposed for both standard and Li doped SiO-C grades to reflect measured capacities. SiO_x materials capacity and volume expansion were modeled and good agreement was found with the literature. Finally 21700 cell internal volumes calculation showed that larger than 30% SiO content can be challenging in an optimized hard casing cell because of larger electrode expansion and limited dead volume available.

Acknowledgment

This work is supported by a public grand overseen by the French National research Agency (ANR) as part of the second “Programme d’investissements d’Avenir” (reference: ANR-15-RHUS-0002). The cell developments described here aim at developing an innovative portable artificial Lung (BioArt-Lung 2020 project).

We would like to express our gratitude to Hitomi Miyawaki, Business manager at Special Functional Products Department of Shin-Etsu Chemical Co., Ltd., and Reiko Sakai, assistant at the Research & Development Department Yokonodaira Laboratory for support with the experimentations.

1 B.A. Johnson, R.E. White /Journal of Power Sources 70 48-54 (1998)
2 J.B. Quinn et al. / Journal of The Electrochemical Society, 165 (14) A3284-A3291 (2018)
3 V. Muenzel et al. / Journal of The Electrochemical Society, 162 (8) A1592-A1600 (2015)
4 A H Tkaczyk et al / J. Phys. D: Appl. Phys. 51 203001 (2018)
5 J. Sturm et al. / Journal of Power Sources 412 204–223 (2019)
6 S. Flandrois, B. Simon / Carbon 37 165 –180 (1999)
7 F Joho et al. / Journal of Power Sources 97-98 78-82 (2001)
8 M. J. Lain et al. / Batteries, 5, 64 (2019)
9 M. N. Obrovac et al. / Journal of The Electrochemical Society, 154 2 A103-A108 (2007)
10 Z.Liu et Al. / Chem. Soc. Rev., 48, 285-309 (2019)
11 A. Yamano et al. / Journal of The Electrochemical Society, 162 (9) A1730-A1737 (2015)
12 K. Schulmeister et al. / Journal of Non-Crystalline Solids 320 143–150 (2003)
13 J. Wang et al. / Journal of Power Sources 196 4811–4815 (2011)
14 W.Wu et al. /Electrochimica Acta187 473–479 (2016)
15 Yamada et al. / Journal of The Electrochemical Society, 159 (10) A1630-A1635 (2012)
16 L Wang et al. / RSC Advances, 3, 15022 (2013)
17 T. Hirose et al. / Solid State Ionics, 303 154–160 (2017)
18 S.H. Kang et al. / Mater Sci 43:4701–4706 (2008)
19 L. Zhang et al. / Journal of Power Sources 400 549–555 (2018)
20 Z. Wang et al. / Journal of Power Sources 260 57-61 (2014)
21 M. Saito et al. / Journal of The Electrochemical Society, 166 (3) A5174-A5183 (2019)
22 D. Shanmukaraj et al. / Electrochemistry Communications 12 1344–1347 (2010)
23 R.W. Grant et al. / US patent US 2015/0191841 Al (2015)
24 T. Hirose et al. / Solid State Ionics 304 1–6 (2017)
25 K.G. Gallagher et al. / Journal of The Electrochemical Society, 163 (2) A138-A149 (2016)
26 J. Cannarella, C.B. Arnold / Journal of Power Sources 245 745-751 (2014)
27 D. Liu et al. / Journal of Power Sources 232 29-33 (2013)
28 S. P.V. Nadimpalli et al. / Journal of The Electrochemical Society, 162 (14) A2656-A2663 (2015)
29 E.M.C. Jones et al. / Journal of The Electrochemical Society, 163 (9) A1965-A1974 (2016)
30 H. Kamo et al. / European patent application EP 3 444 877 A1
31 T. Hirose et al. / European patent application EP 3 467 913 A1
32 M. Marinaro et al. / Journal of Power Sources 357 188-197 (2017)
33 J. Shen et al. / Journal of Electroanalytical Chemistry 834 1–7 (2019)
34 X. Li et al. / Electrochimica Acta 297 1109-1120 (2019)
35 C.C. Nguyen et al. / Journal of The Electrochemical Society, 160 (6) A906-A914 (2013)
36 K.W. Kim et al. / Electrochimica Acta 103 226– 230 (2013)
37 F. Jeschull et al. / Electrochimica Acta 320 (2019) 134602
38 H. Zheng et al. / Electrochimica Acta 71 258– 265 (2012)
39 Freytag et al. / J. Phys. Chem. C, 123, 11362–11368 (2019)
40 Kitada et al. / J. Am. Chem. Soc. 141, 7014–7027, (2019)
41 G. R. Goward, et al. / J. Mater. Chem., 10, 1241 (2000)
42 T. Hirose et al. / Solid State Communications 269 39–44 (2018)
43 Miyachi, et al. / Journal of The Electrochemical Society, 152 (10) (2005)
44 R.Qiao et al. / PLoS ONE 7(11) e49182 (2012)
45 J.-H. Kim et al. / Journal of Electroanalytical Chemistry 661 (2011) 245–249
46 Kim et al. / Journal of The Electrochemical Society, 154 12 A1112-A1117 (2007)
47 K.F Hesse / Acta Cryst. B33,901-902 (1977)
48 C.H Doh et al / Journal of Electrochemical Science and Technology, Vol. 2, No. 3, 146-151 (2011)
49 S.-G. Ma et al. / Materials and Design 118 218–225 (2017)
50 A Yang et al / J. Am. Ceram. Soc., 95 [6] 1818–1821 (2012)
51 Flavors et al. / Sci Rep. Apr 15;4:4605 (2014)
52 S.-S. Suh et al. / Electrochimica Acta 148 111–117 (2014)
53 M. Haruta et al. / Journal of The Electrochemical Society, 166 (2) A258-A263 (2019)
54 H. Takezawa et al. / Journal of Power Sources 244 149-157 (2013)
55 X. Meng et al. / Electrochimica Acta 283 183-189 (2018)
56 H. Takezawa et al. / Electrochimica Acta 245 1005–1009 (2017)
57 M. A. Al-Maghrabi et al. / Journal of The Electrochemical Society, 160 (9) A1587-A1593 (2013)
58 C.C Nguyen et al. / Journal of The Electrochemical Society, 160 (6) A906-A914 (2013)
59 T. Miyuki et al. / Electrochemistry, 80(6), 405408 (2012)
60 K. Pan et al. / Journal of Power Sources 413 20–28 (2019)

61 D. Wainwright et al. / Journal of Power Sources, 34 31-38 (1991)
62 L. de Biasi et al. / J. Phys. Chem. C, 121, 26163−26171 (2017)
63 T. Waldmann et al. / Journal of The Electrochemical Society, 161 (10) A1742-A1747 (2014)
64 A. Pfrang et al. / Journal of Power Sources 392 168–175 (2018)